

Investigation on Flow Characteristics and Performance Estimation of a Hybrid SVC Nozzle

S. Jing-wei[†], W. Zhan-xue, Z. Li, and S. Xiao-lin

Shaanxi Key Laboratory of Internal Aerodynamics in Aero-engine, Collaborative Innovation Center for Advanced Aero-Engine, School of Power and Energy, Northwestern Polytechnical University, Xi'an, Shaan Xi Province, 710072, China

[†]Corresponding Author Email: shijw@nwpu.edu.cn

ABSTRACT

Higher vector efficiency of fluidic thrust vectoring (FTV) technology results in less requirement on secondary flow mass, which helps to reduce the influence of secondary flow on the performance of an aero-engine. In the paper, a new concept of FTV, named as a hybrid shock vector control (SVC) nozzle, was proposed to promote the vector efficiency of a SVC nozzle. It adopts a rotatable valve with a secondary flow injection to enhance the jet penetration, so as to improve the vector performance. The flow characteristics of a hybrid SVC nozzle were investigated numerically by solving 2D RANS equations. The influence of secondary pressure ratio (*SPR*) and rotatable valve angle on vector performance were conducted. Then, the coupling performance of a hybrid SVC nozzle and an aero-engine was estimated, by using the approximate model of a hybrid SVC nozzle and the performance simulation model of an aero-engine. Results show that, a desirable vector efficiency of $2.96^\circ / \%-\omega$ (the vector angle achieved by using secondary flow of 1% of primary flow) of a hybrid SVC nozzle was obtained. In the coupling progress, when a secondary flow of 5.3% of primary flow was extracted from fan exit to a hybrid SVC nozzle, a vector angle of 14.1° , and a vector efficiency of $2.91^\circ / \%-\omega$ were achieved. Meanwhile the thrust of the aero-engine thrust decreased by 5.6% and the specific fuel consumption (*SFC*) increased by 0.5%.

Keywords: Flow characteristics; Transverse injection; Vector performance; Coupling Performance; approximate model.

NOMENCLATURE

A_7	area of nozzle inlet	P_o^*	outer flow total pressure
A_8	area of nozzle throat	P_{ej}^*	ejection flow total pressure
A_9	nozzle exit area	P_{noz}^*	nozzle total pressure
A_s	ratio of secondary injection area to nozzle throat area	P_{sec}^*	secondary flow total pressure
$C_{D,noz}$	mass flow discharge coefficient of nozzle	P_a	ambient static pressure
$C_{D,sec}$	mass flow discharge coefficient of secondary flow channel	R	rotatable valve radius
C_{fg}	nozzle thrust coefficient	<i>SPR</i>	secondary pressure ratio, the ratio of secondary flow inlet total pressure to the ambient pressure
<i>EPR</i>	ejection pressure ratio, the ratio of ejection flow total pressure to the ambient pressure	SVC	shock vector control
$F_{i,ej}$	ejection flow ideal isentropic thrust	T_o^*	outer flow total temperature
$F_{i,noz}$	nozzle ideal isentropic thrust	T_{ej}^*	ejection flow total temperature
$F_{i,sec}$	secondary flow ideal isentropic thrust	T_{noz}^*	nozzle total temperature
FTV	fluidic thrust vectoring	T_{sec}^*	secondary flow total temperature
F_x	X component of thrust	X_j	non-dimensional distance from nozzle throat
F_y	Y component of thrust	y^+	non-dimensional height of first grid near wall
\bar{F}_n	the non-dimensionalized thrust	δ_p	vector angle, \tan^{-1}
J	the ratio of injection jet total pressure to the free stream total pressure	η	vector efficiency
<i>Ma</i>	Mach number	θ	rotatable valve angle
<i>NPR</i>	nozzle pressure ratio, the ratio of nozzle inlet total pressure to the ambient pressure	ω	ratio of air extraction flow to the primary flow

1. INTRODUCTION

The thrust vectoring technology has been emphasized on since 1970s, which is used to enhance the agility and maneuverability, post stall performance, and short take-off and landing of a fighter aircraft (Sehra *et al.*, 2004; Scharnhorst, 2013). It can replace the pneumatic rudder partly or totally to manipulate flight (Gal-Or, 1990), and is considered as a key technology for the fighter aircraft of 4th generation or later. Advanced fighter aircrafts e.g. EP-2000, F-22, SU-35 and F-135 all take advantage of the technology. Nowadays there are two types of thrust vectoring, the mechanical type and fluidic type. The former one has more complex structure and heavier weight, such as the exhaust system of F119 occupying about 30% of the aero-engine weight (Mason *et al.*, 2004), meanwhile other problems of the nozzle gas leaking and heat proofing are more severe. Therefore, the later one came into researchers' consideration, due to its simple structure, low weight, and better reliability over traditional mechanical controlled nozzle (Mason *et al.*, 2004; Weber *et al.*, 1998).

Several types of FTV were investigated in the last two decades, seen in Fig. 1, including co-flow vector nozzle (Heo *et al.*, 2012), counter-flow vector nozzle (Strykowski *et al.*, 1996), throat skewing vector nozzle (Yagle *et al.*, 2000), dual throat vector nozzle (Ferlauto *et al.*, 2017), and shock vector controlling nozzle (Waithe *et al.*, 2003) *etc.* In common, the target of these FTV is using secondary flow to control primary flow of nozzle to deflect and to achieve thrust vectoring. However, because of their different working principles, the thrust vector efficiency, nozzle thrust coefficient ($C_{f\theta}$), and suitable working conditions are different. Among them the SVC method behaves better for exhaust system with high designed nozzle pressure ratio (NPR_D), which can be used on modern aero-engine of high thrust-to-weight ratio, therefore it is paid to more attention.

Presently, flow mechanism, effects of aerodynamic and geometric parameters, and different concepts of a SVC nozzle were investigated numerically and experimentally. Critical parameters e.g. secondary pressure ratio (SPR), secondary injection angle (θ), secondary position (X_j), secondary injection configurations were identified (Waithe *et al.*, 2003; SHI *et al.*, 2016; WANG *et al.*, 2011). Multi-functions concept of SVC was explored. Chiarelli (1993) combined SVC and co-flow concept to get multi-axis thrust vectoring, Anderson (1997) adapted SVC and mechanical method to improve vector performance, and Williams (2002) designed his FAVEN with throttling and vectoring capability.

However, there are two aspects of studies which still need to be considered. On one hand, the SVC

vector efficiency is low, about 0.7-1.4 °/%- ω , which means more secondary flow is needed to be extracted from high pressure components to achieve high vector angle, so augmented SVC concept should be considered and studied. On the other hand, the high-pressure secondary flow from high pressure components for nozzle vector control will alter the operation point of an aero-engine. The evaluating model for the coupling characteristic of the augmented SVC nozzle and aero-engine must be established.

So the work of this paper is based on the problems of the two aspects. Research was conducted on the parts of work. 1) A new concept FTV is proposed, by combining the SVC and a simple mechanical controlled rotatable valve, name a hybrid SVC. Based on 2D CFD, the mechanism and flow characteristics of a hybrid SVC nozzle was studied, focusing on confined space transverse injection, shock wave and vortex characteristic. 2) A method to estimate the coupling performance of a hybrid SVC nozzle and a aero-engine was proposed, using design of experiment (DOE), response surface methodology (RSM), and the aero-engine overall simulation program with air extraction. In the coupling progress, different air extraction positions and extraction ratios were taken into consideration.

2. THE WORKING PRINCIPLE AND NUMERICAL APPROACH

2.1 Working Principle of a Hybrid SVC Nozzle

The thrust vectoring of a SVC nozzle is achieved by injecting a secondary flow into supersonic primary flow at the nozzle divergent section. An obstacle is formed and an oblique shock wave is generated, which deflects primary flow and achieves desirable vector angle. To obtain larger thrust vector angle (e.g. 15°), the energy of secondary flow is usually large, about up to 15% of primary flow energy. It needs a large amount of secondary flow extracted from high pressure component of aero-engine, therefore, a significant effect on the performance of a aero-engine is unavoidable. So how to improve the vector performance of a SVC and how to reduce the secondary flow requirement become research hotspots. Presently, there are many efficient methods proposed in public literatures. One typical case is from Anderson (1997). He studied a mechanical / fluidic thrust vectoring which is ingenious and shows good results on vector performance, however, at afterburning conditions, the thrust efficiency is not improved.

In the paper, a hybrid SVC nozzle is proposed by combining a secondary injection and a rotatable valve, seen in Fig. 2. The key component is the

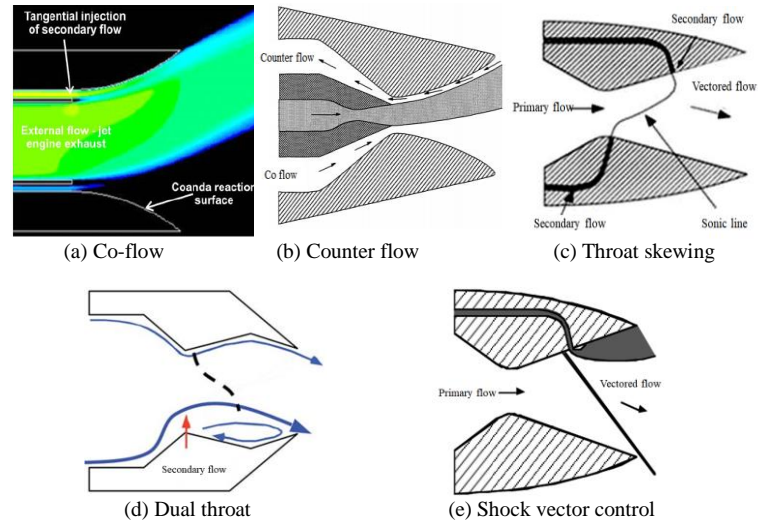


Fig. 1. Different types of fluidic thrust vectoring.

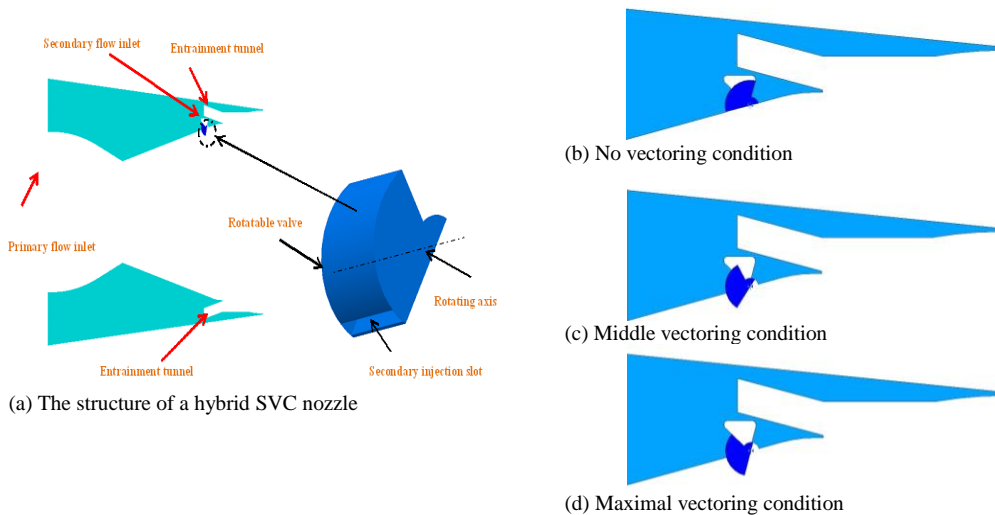


Fig. 2. Sketch of a hybrid SVC nozzle.

rotatable valve, which is installed at the rear part of nozzle divergent section. There are two cylindrical surfaces with different radius which are rotating contact surfaces, and a secondary injection channel in the valve. The radius of cylindrical surfaces, the width of secondary injection slot and the position of the valve are selected according to requirement. When thrust vectoring is required, the valve is rotated and secondary flow is injected, the rotation angle and secondary flow mass rate are the controllable variables. Figs. 2(b), (c) and (d) show typical working conditions with different rotation angles. At (b) condition thrust vectoring is turned off, and at the maximal conditions, (c), the rotatable valve and secondary injection are controlled and desirable thrust vectoring is achieved. From the perspective of rotatable valve structure, the maximal rotation angle should be limited, and in a hybrid SVC nozzle, the maximal rotation angle is 60° . When rotation angle exceeds 60° , the gas leakage occurs, which is not good. Additionally,

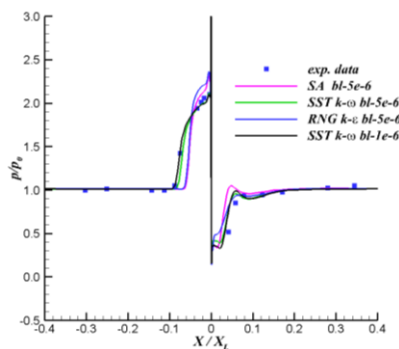
symmetric ejection tunnels are adopted downstream of rotatable valve to alleviate over expansion loss and to improve thrust coefficient at low *NPRs*.

2.2 Simulation Scheme and Turbulence Model

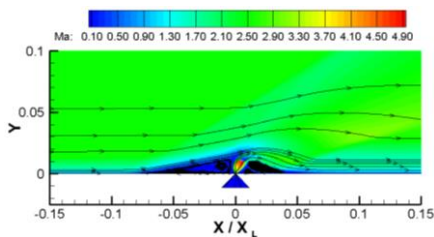
The investigation on flow characteristics of a hybrid SVC nozzle was conducted by using the commercial software of Fluent. The governing equations solved are the two-dimensional, compressible, Reynolds averaged, Navier-Stokes equations, which were discretized in finite volume form on each of the control volumes. The second order upwind scheme was adopted in the spatial discretization, while the second implicit scheme adopted for the time discretization. The implicit density-based algorithm was chosen. The Foe-FDS flux type was used.

The hybrid SVC nozzle has the typical flow fields of transverse sonic jet injected into supersonic flow.

Before the simulation study, the turbulence model must be validated, because in transverse injection flows, turbulence model plays an important role, and different turbulence models behave diversely at different *SPR* conditions. In this paper, the turbulence model was validated by experimental data of [Spaid \(1968\)](#). A typical case which has similar working condition with the hybrid SVC nozzle was chosen. The free stream *Ma* is 2.61 and the ratio of injection jet total pressure to free stream total pressure (*J*) is about 1.15. Different turbulence models, including Spalart-Allmaras model, RNG *k-ε* model, and SST *k-ω* model, were chosen to test the prediction precision. Results are shown in Fig. 3. The *X* coordinate is nondimensionalized by the half length of experiment plane, and the *Y* coordinate in Fig. 3(a) and (b) is nondimensionalized by free stream total pressure and the half length of experiment plane, respectively. As can be seen, the SST *k-ω* with compressible effect predicts wall pressure distributions upstream and downstream of injection slot better. It behaves better when the height of the first layer of grid is about 1×10^{-6} m. Thus, the SST *k-ω* with compressible effect was finally chosen to perform the numerical simulations of a hybrid SVC nozzle.



(a) The comparison of predicted pressure distributions and experimental data



(b) The flow fields predicted by SST *k-ω* turbulence model

Fig. 3. Turbulence model validation using experimental data.

2.3 Geometric Model and Computational Grid

A hybrid SVC method is suitable for a rectangular nozzle which is better for integrating with aircraft. It can reduce the install penalty and the after-body drag. Two dimensional geometric model and two dimensional simulations were chosen in the paper, due to the uniform flow fields in span-wise

direction. The detail geometric parameters of a 2D hybrid SVC nozzle are showed in Fig. 4 and listed in Table 1. The rotatable valve locates at the divergent part of a hybrid SVC nozzle. X_j is the relative position, θ is the rotatable valve angle, and A_s is the secondary injection area.

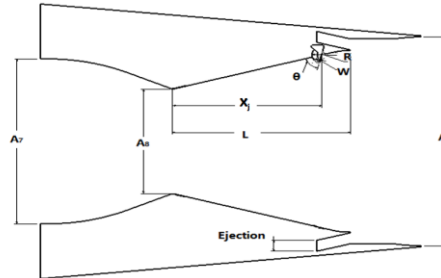
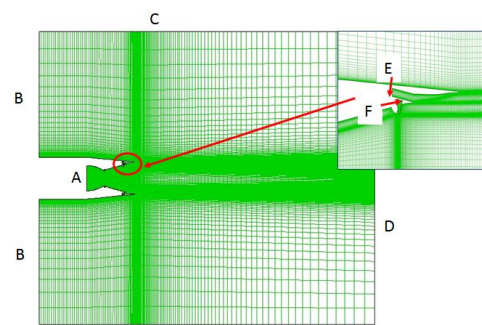


Fig. 4. Geometric model of a SVC nozzle.

Table 1 Design parameters of a hybrid SVC nozzle

<i>NPR_D</i>	Designed <i>Ma</i>	Expansion ratio	Divergent angle(β)/ $^\circ$
10	2.16	2.0	15.0

The structural grid of a hybrid SVC nozzle is seen in Fig. 5. Meshes around injection slot and near nozzle walls are refined. The y^+ of the first layer of grid is about 1.0. Before numerical simulation study, the grid dependence analysis was performed. Three sets of mesh were considered: 150000 cells, 300000 cells and 450000 cells. The results show that the maximum difference in the thrust vector performance is within 1.0%, and the main separation line location almost locates at the same position. Thus the grid of 150000 cells is employed for simulations of a hybrid SVC nozzle.



A: Nozzle inlet, B: outer flow field inlet, C: far field, D: outlet, E: ejection inlet, F: secondary flow inlet

Fig. 5. Computational grid.

2.4 Boundary Conditions

On the boundary of nozzle inlet, secondary flow inlet, ejection flow inlet and outer flow field inlet the total pressure (P_{noz}^* , P_{sec}^* , P_{ej}^* , P_o^*), total temperature (T_{noz}^* , T_{sec}^* , T_{ej}^* , T_o^*) and flow angle are provided. Nozzle pressure ratio (*NPR*),

secondary pressure ratio (*SPR*) and ejection pressure ratio (*EPR*) were used to represent the total pressure of primary flow, secondary flow and ejection flow. *NPR* varies from 4 to 14, *SPR* has a range of 0.6, 0.8, 1.0, 1.2, 1.5, while *EPR* keeps 1.05. The inlet total temperature of secondary flow is related with its total pressure, and it is calculated by Eq. (1).

$$\frac{T_{sec}^*}{T_0} = \left(\frac{P_{sec}^*}{P_0} \right)^{\frac{k}{k-1}} \quad (1)$$

On the boundary of outlet (Fig. 5(D)), the static pressure (P_0) is imposed and the other variables are extrapolated from the interior. On the boundary of pressure-far-field, static pressure, free-stream Ma_∞ of 0.05 and flow direction are provided. Impermeable, no-slip and adiabatic wall boundaries are applied on the solid wall to ensure zero normal flux of mass, momentum and energy crossing the mesh face that lapped with the wall boundary.

2.5 Parameters Definitions

For a hybrid SVC nozzle, three critical parameters are used to estimate its performance: the thrust vector angle (δ_p), the thrust coefficient (C_{fg}), and the vector efficiency (η). The definitions of the performance parameters are as follow:

$$\delta_p = \tan^{-1} (F_y / F_x) \quad (2)$$

In the Eq. (2), F_x and F_y are X and Y components of thrust respectively, which are obtained from Eq. (3) and Eq. (4).

$$F_x = \int_{A_9} (\rho v_x v_x + (p - p_0)) dA \quad (3)$$

$$F_y = \int_{A_9} \rho v_x v_y dA \quad (4)$$

Thrust coefficient is the ratio of actual thrust to ideal thrust, defined in Eq. (5).

$$C_{fg} = F_{noz.} / (F_{i.noz.} + F_{i.sec.} + F_{i.ej.}) \quad (5)$$

Where $F_{noz.}$ is the actual thrust, calculated by equation of $F_{noz.} = \sqrt{F_x^2 + F_y^2}$, and $F_{i.noz.}$, $F_{i.sec.}$ and $F_{i.ej.}$ are ideal thrust of primary flow, secondary flow and ejection flow, calculated by Eq. (6), Eq. (7) and Eq. (8), respectively:

$$F_{i.noz.} = W_{noz.} \sqrt{\frac{2\kappa R}{\kappa-1}} \sqrt{T_{noz.}^* \left[1 - \left(\frac{P_0}{P_p} \right)^{\frac{\kappa-1}{\kappa}} \right]} \quad (6)$$

$$F_{i.sec.} = W_{sec.} \sqrt{\frac{2\kappa R}{\kappa-1}} \sqrt{T_{sec.}^* \left[1 - \left(\frac{P_0}{P_{sec.}^*} \right)^{\frac{\kappa-1}{\kappa}} \right]} \quad (7)$$

$$F_{i.ej.} = W_{ej.} \sqrt{\frac{2\kappa R}{\kappa-1}} \sqrt{T_{ej.}^* \left[1 - \left(\frac{P_0}{P_{ej.}^*} \right)^{\frac{\kappa-1}{\kappa}} \right]} \quad (8)$$

The vector efficiency (η) is defined as the ratio of vector angle to the corrected secondary flow, seen in Eq. (9), and is used to estimate the vector control efficiency of secondary flow on primary flow.

$$\eta = \delta_p / \omega \sqrt{\tau} \times 100\% \quad (9)$$

Where $\omega \sqrt{\tau}$ is the corrected flow ratio of secondary flow, considered by Eq. (10). It is the momentum ratio of secondary flow to primary flow, and indicates the energy needed to achieve thrust vectoring.

$$\omega \sqrt{\tau} = m_{sec.} \sqrt{T_{sec.}^*} / m_{noz.} \sqrt{T_{noz.}^*} \quad (10)$$

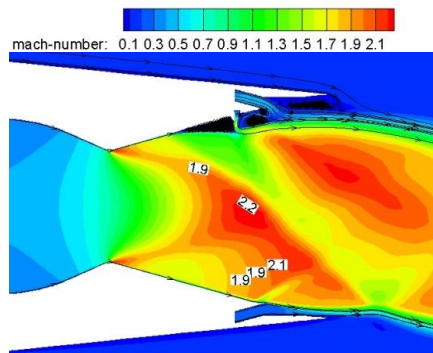
3. RESULTS AND DISCUSSION

3.1 Flow Characteristics of a Hybrid SVC Nozzle

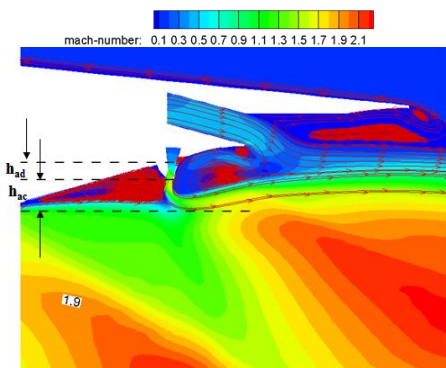
Transverse injection and shock wave / boundary layer interactions are two typical flow phenomenon of a hybrid SVC nozzle. The transverse injection of a secondary flow distributes supersonic primary flow, causes an oblique shock wave and deflects primary flow. The rotatable valve enhances the injection penetration depth and changes trajectory of transverse injection. Therefore, the vector performance of a hybrid SVC nozzle is improved, meanwhile its flow characteristics become more complex.

For a hybrid SVC nozzle with the rotation valve angle of 60° , secondary injection slot width of 8 mm, the basic flow characteristics were investigated at condition of nozzle pressure ratio (*NPR*) of 8.0, secondary pressure ratio (*SPR*) of 1.0 and ejection pressure ratio (*EPR*) of 1.05. *Ma* contours and streamlines are shown in Fig. 6. It is seen that a strong induced shock wave was formed upstream of the rotatable valve due to the disturbance of rotatable valve and secondary injection into supersonic primary flow. The shock wave strength and flow losses are un-uniform, because the *Ma* number distributions upstream of shock wave are different, which ranges from about 1.5 to 2.2 with the maximal *Ma* number locates in the center of nozzle. Strong adverse pressure gradient was caused by shock wave, resulting in the separation of boundary layer upstream of rotatable valve. The separation zone is wedge-shaped. The streamlines direction of recirculation zone is clockwise. The pressure of the separation zone caused by shock waves is relative high and offers unbalanced side-force for primary flow deflection, seen in Fig. 7. Due to the entrainment of high pressure and high speed secondary flow, an anticlockwise recirculation zone is also generated (Fig. 6(b)). The two recirculation zones form a pair of counter rotating vortex, which also contributes to the flow losses. The *Ma* number

of primary flow could reduce to 1.3 when primary flow goes through shock wave, and it increases again after shock wave when primary flow passes an expansion fan over the top of injection trajectory.



(a) The Ma distributions of a hybrid SVC nozzle



(b) Local Ma distributions

Fig. 6. Basic flow characteristics of a hybrid SVC nozzle.

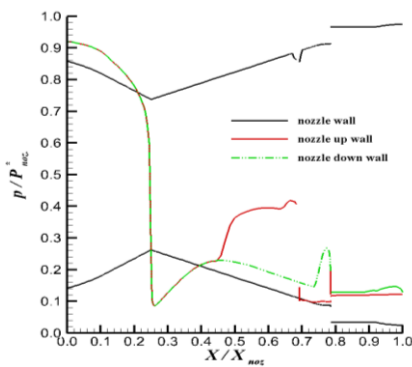


Fig. 7. Pressure distributions on nozzle walls.

As is seen in Fig. 6(a) and (b), Low speed and low pressure zones appear downstream of the rotatable valve. The pressure of ejection flow is higher than the pressure downstream of rotatable valve, and the relatively low pressure made flow of ejection tunnel come into the recirculation zone, which is observed from streamlines distributions. It results in the pressure downstream of rotatable valve increasing. In the recirculation zone three vortices were formed, a large anti-clock one and two small clockwise ones. Ejection flow was then entrained by high speed primary

flow and the large anti-clock vortex appeared as an open separation. The ejection flow at the same side with the rotatable valve deflects with primary flow, therefore another low pressure zone after ejection tunnel was generated. The ambient air flowed into the zone due to the local negative pressure difference, forming a tip vortex and another open separation. Compared with the ejection flow at the same side with rotatable valve, the other ejection flow at the opposite side has simpler flow structures and has less flow losses. For the two ejection flows, the acceleration of the flow at the same side with the rotatable valve is more evident due to a relatively low background pressure, the Ma number is about 0.3, while in the opposite ejection flow the Ma number is about 0.2. The corresponding results are that there is a larger amount of flow in the former ejection tunnel and it is about 50% larger than the other one. From the pressure distributions at nozzle exit (Fig. 8), it can be seen that ejection flows increase static pressure near nozzle wall, and the pressure ratio of upper ejection flow to ambient is about 0.97 while the other ratio is about 1.03. Therefore, the thrust loss due to negative pressure difference is reduced, and thrust coefficient (C_{fg}) increases. In the condition, the C_{fg} is about 0.934.

At the calculation condition, the ratio of secondary flow to primary flow is about 2.12%, while the ejection flow ratio is about 1.96%. A vector angle (δ_p) of 6.27° was finally obtained, and the thrust efficiency of $2.96^\circ/\%-\omega$ was achieved, which means a thrust vector angle of 2.96° is gained by using secondary flow one percent of primary flow. It is much higher than the vector efficiency of a SVC nozzle ($0.7-1.4^\circ/\%-\omega$) (Deere, 2003). It also indicates the advantage of the new concept thrust vectoring method.

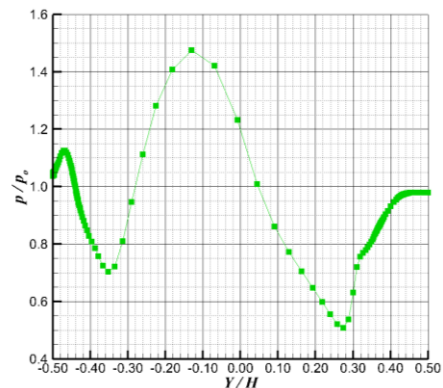


Fig. 8. Pressure distributions at nozzle exit.

Secondary pressure ratio (SPR) and rotatable valve angle (θ) are two critical control variables. By the modification of SPR and θ , continuous vector angles can be achieved.

Influence of SPR on vector performance of a hybrid SVC nozzle was investigated, while other parameters keep constant, i.e. rotation valve angle

of 60° , secondary injection slot width of 8 mm, NPR of 8.0, and ejection pressure ratio (EPR) of 1.05. Different SPR value was considered, including 0.6, 0.8, 1.0, 1.2 and 1.5.

With the increase of SPR , the mass flow and the momentum of secondary flow increased, which enhanced the jet penetration depth of secondary flow and altered flow fields distributions. As is seen in Fig. 9, the induced shock wave moved forwards when SPR increased, and the separation length of boundary layer upstream of the rotatable valve increased. It resulted in larger high pressure zone upstream of the rotatable valve, seen in Fig. 10, and larger side-force for primary flow deflection. That means the vector angle increased with the increase of SPR , seen in Fig. 11. Noticeably, when SPR is 1.5, the boundary layer separation point moved to nozzle throat, and a vector angle of 7.47° was achieved. Additionally, when SPR changed from 0.6 to 1.5, the maximal Ma number upstream of shock wave decreased from about 2.4 to 1.9, therefore, the shock wave strength decreased, which is benefit for thrust coefficient.

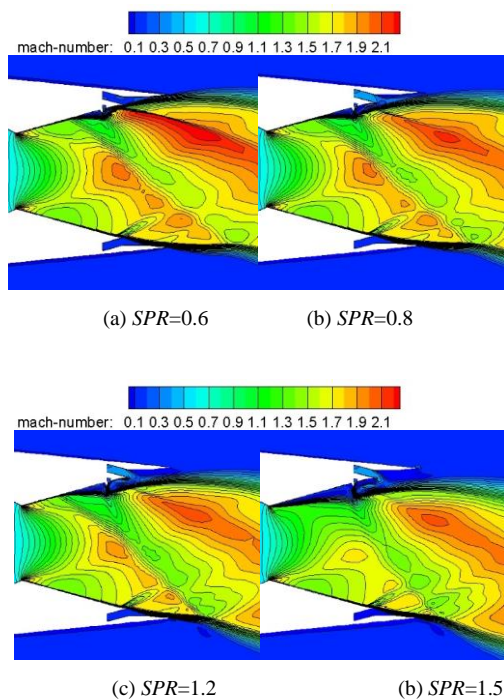


Fig. 9. Ma distributions at different SPR conditions.

The increase of SPR has more evident effect on the flow fields downstream of the rotatable valve. At low SPR of 0.6, the secondary flow attached to nozzle wall, and a closed separation was formed. At the attachment point, a strong reattachment shock wave was generated. It deflected primary flow and brought out flow losses. When SPR increased to 0.80 or larger, the secondary flow did not attach to nozzle wall anymore. Correspondingly, flow separation type changed to open type. The reattachment shock wave weakened and gradually turned to strong compress wave at SPR of 1.5. At

these conditions, ejection flow partly went into the open separation zone and partly deflected with primary flow, which caused a low pressure zone at rear part of nozzle and the ambient air went into this zone and formed a tip vortex and another open flow separation.

The vector efficiency η , a maximum value, 2.34% , was obtained at condition of SPR of 1.5, and a minimum value, 2.12% , was obtained at condition of SPR of 0.6. It is found that when SPR has a wide variable range, the vector angle has a large increase, but the vector efficiency did not change much. It is concerned with the definition of the vector efficiency, seen in Eq. (9), and the changing trend of vector angle and corrected secondary flow. In this study, both the vector angle and secondary flow have approximate linear relationship with SPR . Therefore, the vector efficiency has small change.

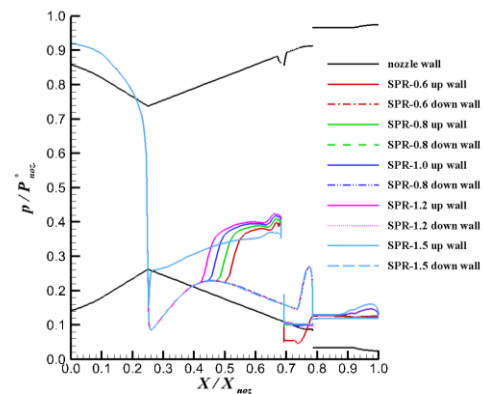


Fig. 10. Pressure distributions on nozzle walls at different SPR s.

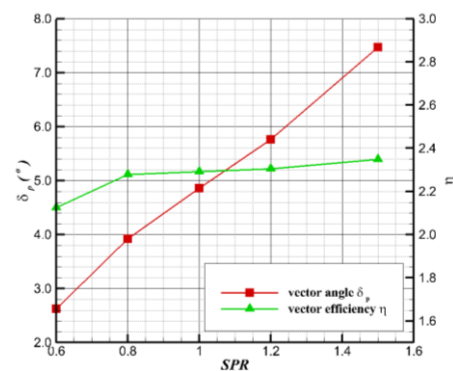


Fig. 11. Vector performance at different SPR s.

Influence of rotatable valve angle (θ) on vector performance of a hybrid SVC nozzle was investigated, while other parameters keep constant, i.e. secondary injection slot width of 8 mm, NPR of 8.0, SPR of 1.0 and ejection pressure ratio (EPR) of 1.05. Different θ value was considered, including 30° , 40° , 50° and 60° .

The rotatable valve is used to provide an auxiliary penetration depth for secondary injection, and is used to control the injection direction of the secondary flow. With the increase of rotatable valve

angle, the auxiliary penetration depth was enhanced and the momentum component of secondary flow normal to primary flow also increased, which is helpful to achieve larger high pressure zone upstream of the rotatable valve. As is seen in Fig. 12 and Fig. 13, the final secondary jet penetration depth gradually increase, which has larger interaction on supersonic flows and induced stronger shock wave. As a result, the boundary layer separation zone enlarged when θ increased from 30° to 60° .

With the increase of θ , there is also a change of separation type downstream of the rotatable valve. The attached secondary flow at condition of θ of 30° turned to detach from nozzle wall when θ exceeded 40° . Therefore, the closed flow separation became open type. And it caused the pressure on nozzle wall downstream of the rotatable valve to increase, seen in Fig. 13.

The vector angle of a hybrid SVC nozzle increased from 2.06° to 4.85° when θ increased from 30° to 60° . Meanwhile the mass flow of secondary flow almost kept constant, therefore, the vector efficiency (η) had an increase too, which increased from $1.70^\circ/\%-\omega$ to $2.29^\circ/\%-\omega$, seen Fig. 14.

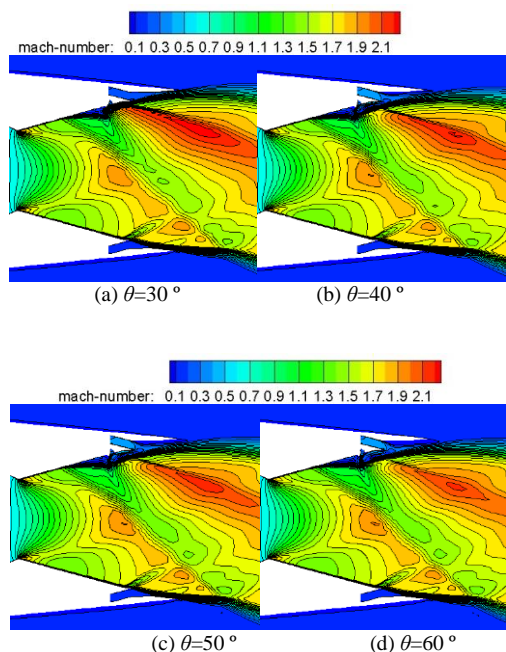


Fig. 12. Ma distributions at different rotatable valve angles.

3.2 Performance Estimation of a Hybrid SVC Nozzle Coupled with an Aero-Engine

The hybrid SVC nozzle needs high pressure secondary flow from compressor or fan to achieve thrust vectoring, therefore, it has influence on the working performance of an aero-engine. How to estimate the effect and to what extent the effect is must be studied and conformed before the usage of a hybrid SVC technology.

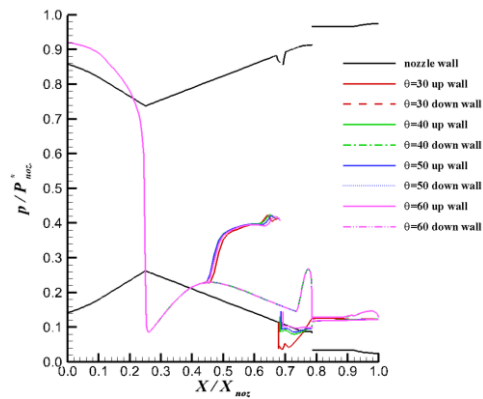


Fig. 13. Pressure distributions on nozzle walls at different rotatable valve angles.

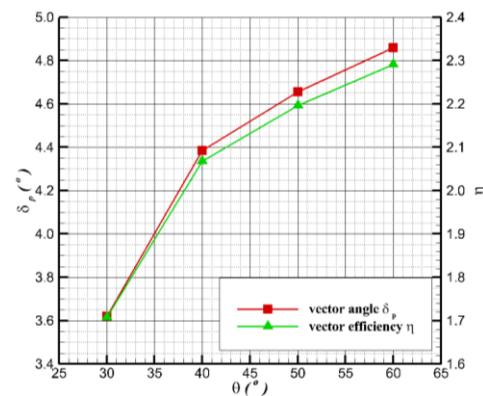


Fig. 14. Vector performance at different rotatable valve angles.

Firstly, the relations and constraints between a hybrid SVC nozzle and an aero-engine should be identified. From the perspective of physical relationship, two mass flow balances must be satisfied. One is the mass flow balance between the nozzle inlet and the aero-engine, the other is mass flow balance between the air extracted from high pressure component (fan, or compressor) of an aero-engine with the secondary flow injected into a hybrid SVC nozzle.

Secondly, the method to obtain the vector performance of a hybrid SVC nozzle needs to be selected. For a Hybrid SVC nozzle, there are about ten parameters affecting its vector performance, including NPR , SPR , nozzle inlet total temperature, secondary inlet total temperature, the area of secondary injection slot, injection angle, the rotation valve angle *etc.* In order to establish a hybrid SVC nozzle database including all the parameters mentioned above to couple with an aero-engine, the number of experiments or simulations is huge. It would take a long time. For the sake of quick obtaining the database of a hybrid SVC nozzle, the approximate models of vector performance were considered, which were accomplished based on a small amount of samples. In the paper, a typical approximate model, response surface methodology (RSM), was used due to its easily obtained polynomial express.

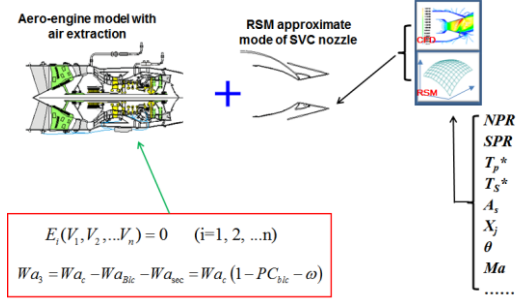


Fig. 15. Method to estimate the coupling performance of a hybrid SVC nozzle and an aero-engine.

For coupling method proposed in this paper (Fig. 15), the response surface methodology (RSM), design of experiment (DOE), CFD and aero-engine simulation program were the basics. The RSM, DOE and CFD were used to obtain the relations between vector performance, e.g. vector angle, nozzle flow coefficient, secondary flow coefficient, etc., and aerodynamic and geometric parameters. Then several approximate models were obtained. The approximated models were brought in the aero-engine simulation mode, generating the coupling model. Therefore, the coupling performances of a hybrid SVC nozzle with an aero-engine can be estimated. The influence of the affecting parameters, the air extraction positions and mass ratios on the vector performance of a hybrid SVC nozzle and the aero-engine / nozzle working performance can be evaluated.

A. The RSM model of a hybrid SVC nozzle

The approximated models established by RSM are the system response functions P_j on design factors X_i , which are based on DOE and polynomial regression or neural networks training *etc.* The DOE provides the sample points, at which the experimental tests or CFD simulations are conducted. The polynomial regression or neural networks training are the method used to obtain the response functions.

For RSM response functions, the polynomials are usually used, because of its accessible expressions and credible accuracy. Before the process, the order and shape should be confirmed. Generally, a first- or second order polynomial is selected, seen as follow:

$$P_j = \beta_0^j + \sum_{i=0}^n \beta_i^j X_i + \sum_{i=0}^n \beta_{ii}^j X_i^2 + \sum_{i \neq k}^n \beta_{ik}^j X_i X_k \quad (11)$$

The polynomial coefficient β_0^j , β_i^j , β_{ii}^j and β_{ik}^j are determined by means of a standard least-square regression which minimizes the sum of the square of the deviations of the predicted values from the actual ones. The validity of established approximate models are verified by different parameter, e. g. R^2 (the ratio of the model sum squares to total sum of squares) and R^2_{adj} (R^2 adjusted to the number of parameters in the model).

In the paper, the processes to obtain the response

functions of a hybrid SVC nozzle are arranged as follow:

- 1) Conforming the design space and variables range. Base on the previous study on influence of designed parameters on the vector performance of a hybrid SVC nozzle, six critical parameters were selected, including *NPR*, *SPR*, secondary injection with, rotatable valve radius, rotatable valve position and rotatable angle.
- 2) Determining the DOE method and generating sample points. The Box-Behnke design (BBD) considering rotatory was finally chosen. Three levels of each parameter were used, seen in Table 2. A sample with 54 points was made, and the center point repeats five times.
- 3) Obtaining response variables. The CFD simulation work was conducted on the 49 sample points, and the response variables of δ_p , C_{fg} , $C_{D.noz}$ and $C_{D.sec}$ were calculated at each point.
- 4) Selecting the type of response function and obtaining coefficients of target functions. The two order polynomial with one order interaction effect was selected as the type of RSM target functions. And the method of standard least-square was used to get the coefficients of target functions. Then the step regress was adopted to filtrate the factors which have faint influence on the response functions, and the polynomial coefficients are updated.
- 5) Evaluating the accuracy of the response functions. R^2 was used to estimate the accuracy of the response functions. If R^2 is larger than 0.75, the response function is good, and it can be used in the later coupling progress. If it is less than 0.75, modify the design space and repeat step 1) to step 5).

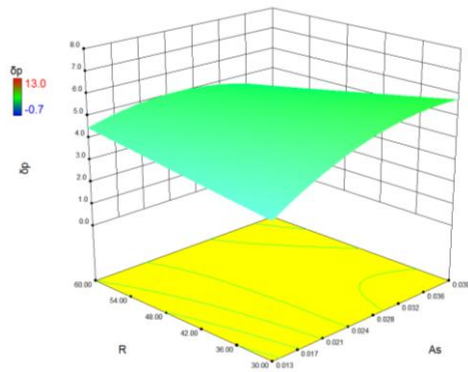
Table 2 Design space of RSM

<i>NPR</i>	<i>SPR</i>	A_s (mm)	R (mm)	X_j	θ (°)
4	0.6	5	30	0.60	30
9	10.5	10	34	0.75	45
14	1.5	15	60	0.90	60

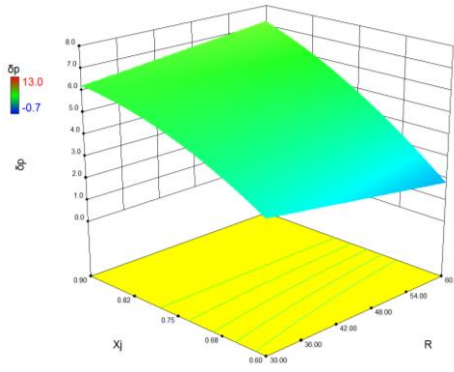
Table 3 Results of R^2

	δ_p	C_{fg}	$C_{D.noz}$	$C_{D.sec}$
R^2	0.975	0.91	0.94	0.95

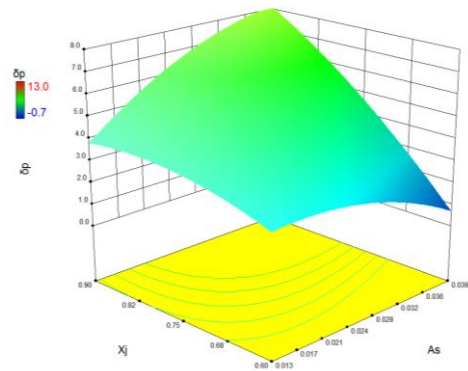
The R^2 of the four response functions of δ_p , C_{fg} , $C_{D.noz}$ and $C_{D.sec}$ were obtained and shown in Table 3. It can be seen that the R^2 of all the response functions are larger than 0.9, which indicates the four approximate models satisfy accuracy requirement and can be used in later research work. Interaction effects of different variables on the response functions cannot be ignored. Two response variables, δ_p and C_{fg} , were focused on, which represents the vector performance and flow loss



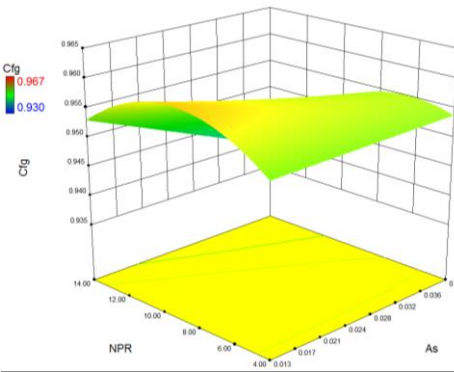
(a) Interaction effect of A_s and R on δ_p



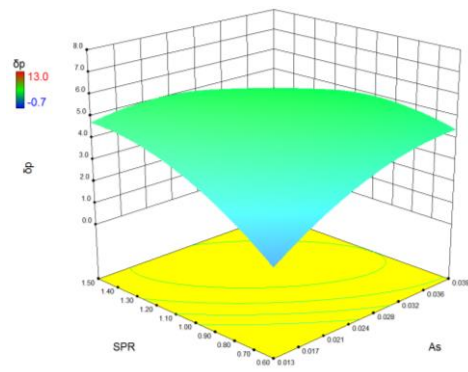
(d) Interaction effect of R and X_j on δ_p



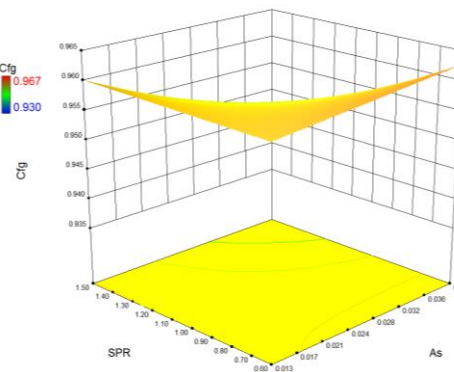
(b) Interaction effect of X_j and A_s on δ_p



(e) Interaction effect of A_s and NPR on C_{f_g}



(c) Interaction effect of SPR and A_s on δ_p



(f) Interaction effect of A_s and SPR on C_{f_g}

Fig. 16. Interaction effects of critical parameters.

characteristics of the hybrid SVC nozzle. As can be seen in Fig. 16, the changing rule of the response function versus one factor and two factors can be totally different. Taking δ_p v.s. secondary injection area (A_s) and rotatable valve radius (R) for example, seen in Fig. 16(a), when R is smaller, with the increase of A_s , δ_p increases to the maximal value then decreases, but when R is larger, δ_p increases with the increase of A_s all along. Other variables, rotatable valve position (X_j) and A_s , secondary pressure ratio (SPR) and A_s , have similar interaction effects on δ_p . The interaction effect of R and X_j of on δ_p is a bit different. At smaller X_j ,

when R increases, δ_p increases, but at larger X_j , when the R increases, δ_p decreases. The similar interaction effect is A_s and SPR on C_{f_g} .

B. Aero-Engine Model with Air Extraction

The aero-engine working characteristics is simulated by solving the co-working balance equations, which are based on the thermodynamic coupling of components, e. g. the power balance of the compressor and the turbine, the pressure and mass flow balance of different components. Generally the equations can be expressed as follow:

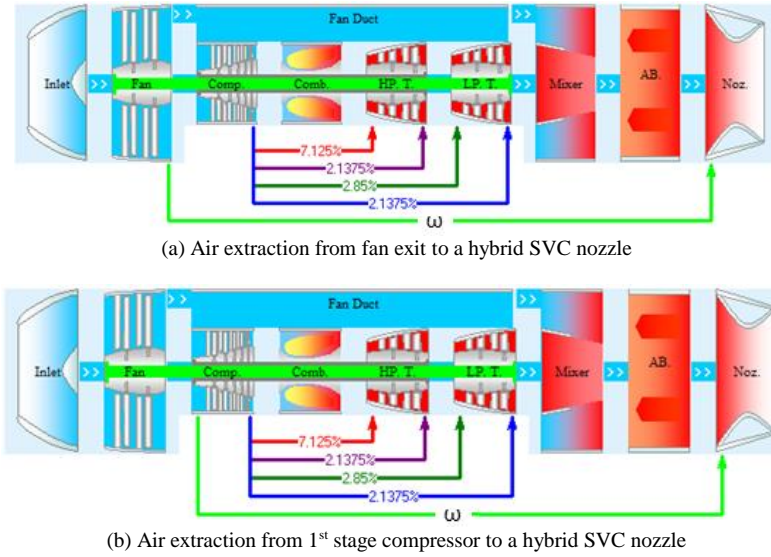


Fig. 17. Models of a Hybrid SVC Nozzle Coupled with an Aero-Engine.

$$E_i(V_1, V_2, \dots, V_n) = 0 \quad (i = 1, 2, \dots, n) \quad (12)$$

V_i represents the of variable for aero-engine simulation. If the character maps of each component are available and controlling principle of aero-engine is provided, the equations can be solved. The performance of the aero-engine and aerodynamic parameters of each section can be obtained.

When secondary flow is extracted from high pressure component, e.g. fan or compressor, the previous balanced relationships must be changed, and the thermal circulation parameters of each component of the aero-engine change accordingly. These changes are expressed by the modification of the outflow of fan or compressor. Taking air extraction from a compressor for example, if the extracted air is ω of total mass flow of a compressor, the mass flowing out of a compressor for the mass balance between a compressor and a combustor changes from Eq. (13)

$$Wa_3 = Wa_c - Wa_{Blc} = Wa_c (1 - PC_{blc}) \quad (13)$$

to Eq. (14).

$$Wa_3 = Wa_c - Wa_{Blc} - Wa_{sec} = Wa_c (1 - PC_{blc} - \omega) \quad (14)$$

The expression of power of a compressor is changed as follow:

$$N_c = m_3 (h_3 - h_2) + m_{ble} (h_{ble} - h_2) + m_s (h_s - h_2) \quad (15)$$

Where N_c is compression power of a compressor, h is the total enthalpy, and the subscripts of 2, 3, ble and s represent the flow in and out of a copressor, the bleeding air and the secondary flow, respectively. When air extraction is from fan, the expressions of mass and power are similar.

Other co-working balanced equations of the aero-

engine are unchanged. And together with the changed balance equations, they are solved by Newton—Raphson iteration method.

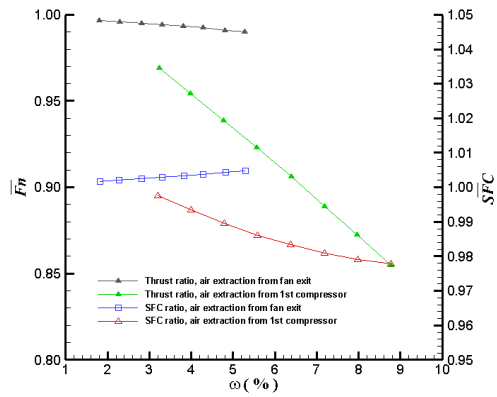
C. The Estimation of Coupling Performance of a Hybrid SVC Nozzle and An Aero-Engine

The interfaces between a hybrid SVC nozzle and an aero-engine must be confirmed, before the coupling performance was estimated. In the paper, there is an additional interface between a hybrid SVC nozzle and an aero-engine, i.e. the secondary flow interface which is between air extraction from high pressure components of an aero-engine and the secondary injection, except the interface of nozzle inlet and turbine exit of an aero-engine. Therefore, there is a variable, the ratio of air extraction, added to the cycling variables which affect the co-working point of an aero-engine.

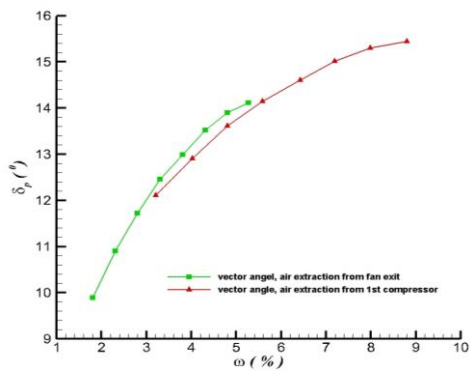
Generally, in physical relationships, the coupling model need to satisfy the mass balance between nozzle and low pressure turbine, and the mass balance between the air extraction from a fan or compressor and the secondary flow injected into a hybrid SVC nozzle for thrust vectoring control.

To establish the coupling model of a hybrid SVC nozzle with an aero-engine, the following steps are followed:

- 1) The air extraction ratio ω was selected as a control variable, while other geometric parameters of a hybrid SVC nozzle were kept constant. The area of the secondary injection slot (A_s) was selected as an iterative variable. In order to meet the mass balance between air extracted from a fan or compressor and the secondary injection, several iterations were conducted. When mass balance was achieved, the A_s was obtained.
- 2) To achieve the mass balance of a hybrid SVC nozzle and an aero-engine, the approximate



(a) Performance of aero-engine



(b) Thrust vector angles

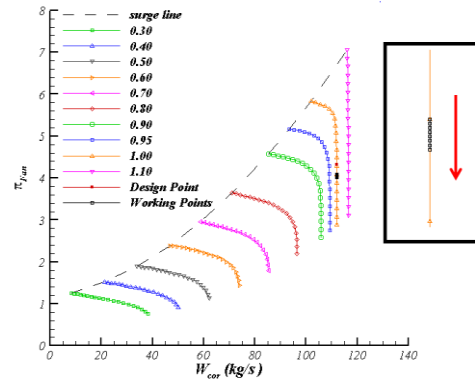
Fig. 18. Coupling performance of a hybrid SVC nozzle and an aero-engine.

models of C_{fg} and C_{Dnoz} from RSM were used, and together with the new equations, Eq. (14) and Eq. (15), the co-operating performance of an aero-engine was solved.

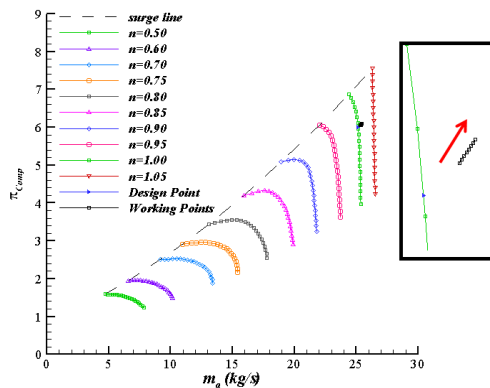
- 3) Different ω and air extraction positions, including fan exit, and 1st stage compressor were considered, shown in Fig. 17. For each coupling model, thrust vector angle (δ_p) and aero-engine performance are evaluated.

In order to make sure SPR ranges from 0.6 to 1.5, the air extraction was arranged in proper positions. As is calculated, it is found that the total pressure of fan exit plane and 1st stage of compressor meet the range well. Therefore, these two positions are considered in the paper. In the coupling progress, the simulation conditions are set as follow: the secondary injection area (A_s) is from 5.0 mm to 15 mm, the rotatable angle θ is 60°, the rotatable valve position X_j is 0.90, the rotatable valve radius is 60mm, the air extraction ratios are from fan exit and 1st stage compressor 1.8%-5.3% and 3.2% to 8.8%, respectively, and the aero-engine works at maximum condition at sea level.

Figure 18 shows the coupling performance of a hybrid SVC nozzle and an aero-engine. When air is extracted from fan exit, with the increase of air extraction ratio (ω), thrust decreases, specific fuel consumption (SFC) increases and thrust vector angle (δ_p) increases. At ω of 5.3%, a decrease of



(a) Influence on working point of fan



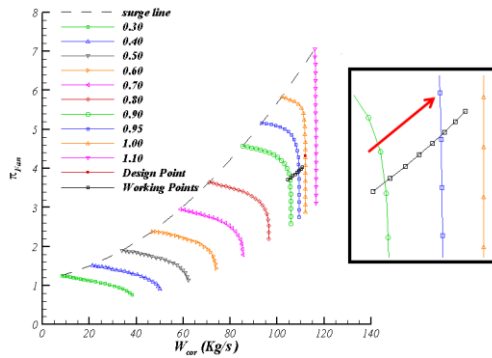
(b) Influence on working point of compressor

Fig. 19. Air extraction from fan exit.

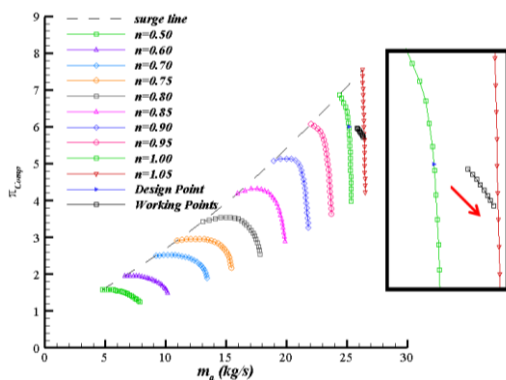
5.6% on thrust, an increase of 0.5% on SFC , and δ_p of 14.1 ° were obtained, and the thrust vectoring efficiency is 2.66 %/%. When air is extracted from 1st stage compressor, thrust decreases rapidly, and SFC increases evidently. At ω of 8.8%, thrust has a decrease of 18%, SFC has a decrease of 3% and δ_p is about 15.5°. The different varying trend of SFC under different air extraction positions is related with mass flow of core-engine and the thrust. When air is extracted from fan, under the engine control principle of constant turbine inlet total temperature, fuel mass flow is almost unchanged, with the decrease of thrust, the SFC will increase. When secondary flow is extracted from 1st stage of compressor, the flow mass of core-engine decreases quickly. At the restriction of constant turbine inlet total temperature restriction, the fuel consumption of combustor decreases rapidly. And results show that the fuel consumption decreases faster than the thrust, therefore, SFC has a trend of decrease. Comparing the influence of different air extraction positions on co-working characters of aero-engine, it can be seen in Fig. 18 and Fig. 19, when secondary flow is extracted from fan exit, the influence is smaller and the working point on map of fan and compressor moves slightly. But when air is extracted from 1st state compressor, significant influence can be witnessed, working point of fan moves to left side while that of compressor move to stall surge. Though extracting air from 1st stage compressor, benefit of SFC and larger vector angle

can be obtained, the thrust decrease dramatically. Therefore, secondary flow extracting from fan exit maybe a better choice.

Influence of other parameters, e.g. the rotatable valve angle, the rotatable valve position, on the coupling performance also can be conducted by the same way and same coupling model, which will be discussed in the late paper.



(a) Influence on working point of fan



(b) Influence on working point of compressor

Fig. 19. Air extraction from 1st stage of compressor.

4. CONCLUSION

A hybrid SVC concept was proposed by combining SVC and a rotatable valve to increase vector efficiency and to decrease the influence on the co-working character of an aero-engine. The working principle was discussed, the flow mechanism of a hybrid SVC nozzle was investigated numerically by 2D CFD, and a method for estimating the coupling performance of a hybrid SVC nozzle and an aero-engine was studied. Conclusions are drawn as follow:

- 1) The internal flow of a hybrid SVC nozzle has the characteristics of confined transverse injection and shock wave / boundary layer interactions. The rotatable valve enhanced the jet penetration depth and increased the ability to deflect supersonic primary flow. It can improve vector efficiency largely. A desirable vector efficiency of $2.96^\circ / \%-\omega$ was obtained, which is

obviously larger than $1.4^\circ / \%-\omega$, the vector efficiency of a SVC nozzle.

- 2) The approximate models of δ_p , C_{fg} , $C_{D.noz}$ and $C_{D.sec}$ on six aerodynamic and geometric factors were established base on DOE, CFD, and RSM. The accuracy of approximate models was acceptable which can be used in coupling progress. And the interaction effects of different parameters were identified.
- 3) New balance equations were proposed for the coupling simulation, and coupling estimation models were established by combining the approximate models and the aero-engine simulation model with air extraction. In the coupling progress, it behaves better when air is extraction from fan exit than that from 1st stage of compressor. For air extraction from fan exit, a vector angle of about 14.1° was achieved, while ω was 5.3% and thrust decreased was within 6%.

ACKNOWLEDGEMENTS

The authors would like to express their gratitude for the financial support of the Fundamental Research Funds for the Central Universities (No.3102017-zy009) and the National Natural Science Foundation of China (No.51576163, No.51876176)

REFERENCES

Anderson, C. J., V. J. Giuliano and D. J. Wing (1997). Investigation of hybrid fluidic/mechanical thrust vectoring for fixed exit exhaust nozzle. *33rd Joint Propulsion Conference and Exhibit*, July 6-9, 1997 Seattle, WA, AIAA 97-3148.

Chiarelli, C. and K. Raymond (1993). Fluidic scale model multi-plane thrust vector control test results. *AIAA/SAE/ASME/ASEE 29th joint propulsion conference and exhibit*, June 28-30, 1993, Monterey, CA. AIAA-93-2433.

Deere, K. A. (2003). Summary of fluidic thrust vectoring research conducted at NASA Langley Research Center[R], AIAA 2003-3800.

Ferlauto, M. and R. marsilio (2017). Numerical investigation of the dynamic characteristics of a dual throat nozzle for fluidic thrust vectoring. *AIAA Journal* 55(1), 86-98.

Gal-Or, B. (1990). The fundamentals concepts of vectored propulsion. *Journal of Power and Propulsion* 6(6), 747-757.

Heo, J. Y. and H. G. Sung (2012). Fluidic thrust-vector control of supersonic jet using coflow injection. *Journal of propulsion and power* 28(4), 858-861.

Mason, M. S. and W. J. Crowther (2004). Fluidic thrust vectoring for low observable air vehicle, 2nd AIAA flow control conference, 28 June-1 July 2004, Portland, Oregon, AIAA

- 2004-2210.
- Scharnhorst, R. K. (2013). Characteristics of future military aircraft propulsion systems. *AIAA* 2013-0466.
- Sehra, A. K. and W. Jr. Woodrow (2004). Propulsion and power for 21st century aviation. *Progress in aerospace sciences* 40(4-5), 199-235.
- Shi, J. W., L. Zhou, Z. X. Wang and X. L. Sun (2016). Investigation on flowfield characteristics and performance of shock vector control nozzle based on confined transverse injection. *Journal of Engineering for Gas Turbines Power* 138(10), 101502-101502-11.
- Spaid, F. W. and E. E. Zukoshi (1968). A study of the interaction of gaseous jets from transverse slot with supersonic external flows. *AIAA Journal* 6(2), 205-212.
- Strykowski, P. J., A. Krothapalli and D. J. Forliti (1996). Counterflow thrust vectoring of supersonic jets. *AIAA Journal* 34(11), 2306-2314.
- Waithe, K. A. and K. A. Deere (2003). Experimental and computational investigation of multiple injection ports in a convergent-divergent nozzle for fluidic thrust vectoring. *AIAA*, 3802, 2003.
- Wang Z. X., Y. N. Wang and Z. J. Li (2011). Experimental on fluidic thrust-vectoring nozzle based on shock control concept. *Journal of propulsion technology* 31(6), 751-756.
- Weber, Y. S. and D. L. Bowers (1998). Advancements in exhaust system technology for the 21st century, *AIAA* 98-3100.
- Williams, R. G. (2002). Fluidic thrust vectoring and throat control exhaust nozzle. *AIAA*, 4046, 2002.
- Yagle, P. J., D. N. Miller and K. B. Ginn (2000). Demonstration of fluidic throat skewing for thrust vectoring in structurally fixed nozzle. *ASME* 2000-GT-0013.